AIP | The Journal of Chemical Physics

Study of C6 − and C6 with threshold photodetachment spectroscopy and autodetachment spectroscopy

Caroline C. Arnold, Yuexing Zhao, Theofanis N. Kitsopoulos, and Daniel M. Neumark

Citation: The Journal of Chemical Physics **97**, 6121 (1992); doi: 10.1063/1.463722
View online: http://dx.doi.org/10.1063/1.463722
View Table of Contents: http://scitation.aip.org/content/aip/journal/jcp/97/9?ver=pdfcov
Published by the AIP Publishing

Articles you may be interested in

Reply to Comment on: Study of C− 6 and C6 with threshold photodetachment spectroscopy and autodetachment spectroscopy
J. Chem. Phys. **99**, 1442 (1993); 10.1063/1.465340

Comment on: Study of C− 6 and C6 with threshold photodetachment spectroscopy and autodetachment spectroscopy
J. Chem. Phys. **99**, 1440 (1993); 10.1063/1.465339

Threshold photodetachment spectroscopy of C− 5
J. Chem. Phys. **95**, 5479 (1991); 10.1063/1.461664

Laser optogalvanic photodetachment spectroscopy: A new technique for studying photodetachment thresholds with application to I−
J. Chem. Phys. **78**, 646 (1983); 10.1063/1.444805

Photodetachment spectroscopy of C2 − autodetaching resonances
J. Chem. Phys. **73**, 4419 (1980); 10.1063/1.440678

This article is copyrighted as indicated in the article. Reuse of AIP content is subject to the terms at: http://scitation.aip.org/termsconditions. Downloaded to IP: 129.174.21.5 On: Wed, 24 Dec 2014 14:15:05

Study of C_6^- and C_6 with threshold photodetachment spectroscopy and autodetachment spectroscopy

Caroline C. Arnold,[a] Yuexing Zhao, Theofanis N. Kitsopoulos,[b] and Daniel M. Neumark[c]
Department of Chemistry, University of California, Berkeley, California, 94720 and Chemical Sciences Division, Lawrence Berkeley Laboratory, Berkeley, California 94720

(Received 19 June 1992; accepted 27 July 1992)

The C_6^- anion and C_6 neutral have been studied using both threshold photodetachment (zero electron kinetic energy) spectroscopy and autodetachment spectroscopy of C_6^-. The threshold photodetachment spectrum yields the electron affinity of linear C_6 to high accuracy, along with the three symmetric stretch frequencies for linear C_6 and the spin–orbit splitting in the ground $^2\Pi_u$ state of the anion. Two of the symmetric stretch frequencies are significantly lower than previous *ab initio* predictions. A simple model force field is used to calculate stretching force constants and estimate bond length changes between the anion and neutral. In addition, using autodetachment spectroscopy, we have located an excited electronic state of C_6^- that lies 43 cm^{-1} below the detachment threshold. This state is very similar in geometry to neutral C_6. Excited vibrational levels of this state autodetach with rates that depend strongly on the available autodetachment channels. The excited state is tentatively assigned to a valence state, rather than an electrostatically bound state.

I. INTRODUCTION

Elemental carbon clusters have been the subject of considerable experimental and theoretical research because of their importance in combustion[1] and astrophysics.[2] The state of carbon cluster research up to 1989 is described in an excellent review article by Weltner and Van Zee.[3] Prior to 1989, most of our knowledge regarding the structure and spectroscopy of small carbon clusters was from *ab initio* calculations. Experimentally, rotationally resolved spectra had only been obtained for C_2 (Ref. 4) and C_3;[5] results for the larger carbon clusters (4–10 atoms) were limited to several matrix isolation studies[6–8] and a photoelectron spectroscopy study of carbon cluster anions.[9] However, during the last three years, new experiments have dramatically increased our understanding of the spectroscopy and structure of these species. For example, Saykally and co-workers[10] have measured gas phase, rotationally resolved infrared spectra for C_3, C_4, C_5, C_7, and C_9, yielding rotational constants and vibrational frequencies; Amano, Bernath, and co-workers[11,12] have also obtained high resolution spectra for several of these species. All of the species observed in these gas phase studies appear to be linear.

Negative ion photodetachment provides another powerful experimental probe of carbon clusters. Although these experiments are typically lower resolution than infrared absorption, they offer several important advantages. One can mass select the anion prior to spectroscopic investigation, eliminating any ambiguity concerning species identification. This is important in cluster studies as most cluster sources simultaneously generate a number of different species (anions, neutrals, and cations). In addition, photodetachment tends to result in excitation of totally symmetric vibrational modes of the neutral. With sufficient resolution, one can determine the frequencies of these modes. Since these are not infrared active for linear molecules, the information obtained is complementary to infrared absorption experiments.

Photoelectron spectra of the carbon cluster anions C_n^- ($n=2$ through 29) have been obtained by Smalley and co-workers,[9] and considerably higher resolution spectra (60–100 cm^{-1}) have been measured for C_2^- and C_3^- by Lineberger,[13,14] and for C_2^- through C_{11}^- by our group.[15] These studies show that the linear even clusters have higher electron affinities than the odd clusters, in agreement with the prediction of Pitzer and Clementi.[16] The higher resolution studies also yielded numerous vibrational frequencies for the neutral clusters. Finally, we have studied C_5^- at even higher resolution using threshold photodetachment spectroscopy.[17] The resolution of this technique is 3–8 cm^{-1}, and the resulting spectrum shows well-resolved transitions to various symmetric stretch and bending modes of C_5, as well as fine structure due to the spin–orbit splitting in the anion.

This paper describes new experiments on the photodetachment spectroscopy of C_6^-, the goal of which is to learn about the structure and spectroscopy of C_6 and C_6^-. Several calculations have been performed on neutral C_6 predicting close-lying cyclic $^1A_1'(D_{3h})$ and $^3\Sigma_g^-(D_{\infty h})$ linear states, although the true ground state remains a point of controversy.[18,19] Raghavachari[18] and Martin[20] have calculated vibrational frequencies for the cyclic and linear isomers, respectively. Calculations performed on the anion have predicted a linear $^2\Pi_u$ ground state.[21] Adamowicz[22] has predicted the existence of several low-lying electronic states of linear C_6^-.

Experimentally, several infrared absorption studies have been performed on C_6 in a low temperature, rare gas

[a] NSF Predoctoral Fellow. Previous name: Caroline J. Chick.
[b] Current address: Combustion Research Facility, Sandia National Laboratories, Livermore, California 94551.
[c] NSF Presidential Young Investigator and Camille and Henry Dreyfus Teacher–Scholar.

 0021-9606/92/216121-15$006.00 © 1992 American Institute of Physics

This article is copyrighted as indicated in the article. Reuse of AIP content is subject to the terms at: http://scitation.aip.org/termsconditions. Downloaded to IP: 129.174.21.5 On: Wed, 24 Dec 2014 14:15:05

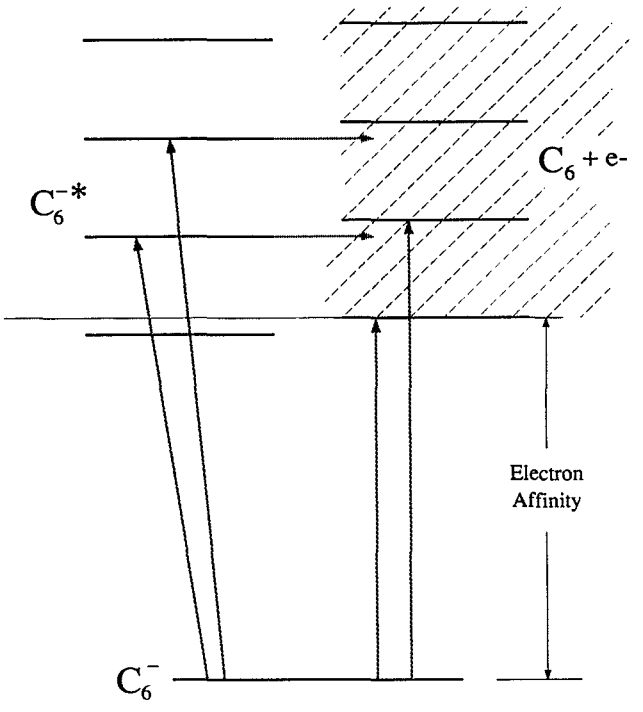

FIG. 1. Energy level diagram illustrating autodetachment and threshold photodetachment transitions. The transitions to the neutral levels yield the zero-kinetic-energy electrons [Eq. (1)] and the transitions to the excited anion levels are followed by autodetachment [Eq. (2)].

matrix.[6,23] The assignment of the observed lines to C_6 antisymmetric has been problematic; only recently, with extensive isotopic substitution, has a line at 1952 cm^{-1} been definitively assigned to a C_6 antisymmetric stretch.[23] Electron spin resonance (ESR) studies[24] in rare gas matrices have shown that linear C_6 in a $^3\Sigma$ state exists, and that the bonding is cumulenic, in accordance with the prediction of Ref. 16. Experimental information on the anion comes from the aforementioned photoelectron spectroscopy studies.[9,15] In addition to yielding the electron affinity of linear C_6, 4.185 ± 0.006 eV,[15] the main features in these spectra were assigned to transitions between linear C_6^- and C_6. However, a high energy "tail" in our C_6^- spectrum was tentatively attributed to a high energy cyclic isomer of the anion. Coulomb explosion measurements also suggest the existence of a cyclic C_6^- isomer.[25]

The results reported here on C_6^- are from two techniques: negative ion threshold photodetachment spectroscopy [zero electron kinetic energy (ZEKE) spectroscopy] and autodetachment spectroscopy. Figure 1 illustrates the energetics of both techniques. In threshold photodetachment spectroscopy, the anions are photodetached with a tunable laser, and the near-zero kinetic energy electron signal is collected as a function of laser frequency. These threshold electrons are produced only when the laser is resonant with an anion→neutral transition

$$C_6^-(v'') + h\nu \rightarrow C_6(v') + e^-(eKE \approx 0). \quad (1)$$

By this means, we can map out the direct photodetachment

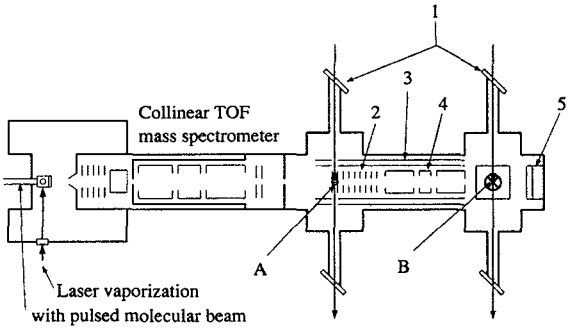

FIG. 2. Diagram of the tunable photodetachment instrument: (A) interaction region for the threshold photodetachment experiment; (B) interaction region for the total cross section experiment; (1) detachment windows; (2) electron extraction plates; (3) magnetic shielding; (4) electron Einzel lens; (5) ion detector. Electron detector is located directly above the circled "X."

transitions between the C_6^- ground state and various vibrational (and electronic) levels of neutral C_6 with 3 cm^{-1} resolution.

In contrast, autodetachment spectroscopy[26] is sensitive to transitions between the ground and excited electronic states *of the anion*. The autodetachment spectrum of C_6^- is obtained by measuring the total photodetachment cross section as a function of the detachment laser frequency. In the absence of anion excited states (the usual case), the photodetachment cross section rises monotonically above the detachment threshold, although in favorable cases one can observe steps in the cross section when new anion→neutral transitions become energetically accessible.[27] However, if there are long-lived excited states of the anion, $(C_6^-)^*$, just above the detachment threshold, the photodetachment cross section will exhibit sharp peaks resulting from excitation to the metastable $(C_6^-)^*$ state followed by autodetachment to the neutral plus electron

$$C_6^- + h\nu \rightarrow (C_6^-)^* \rightarrow C_6 + e^-(eKE \neq 0). \quad (2)$$

The combination of threshold photodetachment spectroscopy and autodetachment spectroscopy has been applied previously to Au_2^- and Au_6^- by Kaldor and coworkers.[28,29]

The threshold photodetachment results presented below show well-resolved transitions between linear C_6^- and C_6, and yield the symmetric stretch frequencies for C_6. In addition, the photodetachment cross section results show sharp autodetachment peaks, indicating that there is an excited electronic state of C_6^- near the detachment threshold. The vibrational frequencies of this anion state are very similar to those of neutral C_6. While C_2^- is known to undergo autodetachment,[26] our results are the first such observation for a polyatomic carbon cluster anion.

II. EXPERIMENT

Figure 2 shows a schematic top view of the apparatus employed for all of the experiments reported in this paper. The machine is described in detail elsewhere,[30] but the basic operation is as follows. Cold carbon clusters (anions,

This article is copyrighted as indicated in the article. Reuse of AIP content is subject to the terms at: http://scitation.aip.org/termsconditions. Downloaded to IP: 129.174.21.5 On: Wed, 24 Dec 2014 14:15:05

cations, and neutrals) are generated in a laser vaporization/pulsed molecular beam source similar to that developed by Smalley.[31] Helium is used as the carrier gas, typically with a backing pressure of 90 psi. Laser vaporization is achieved by focusing a 4 mJ, 532 nm pulse from a frequency-doubled Nd:YAG laser (20 Hz repetition rate) onto a rotating, translating graphite rod (higher pulse energies resulted in significantly hotter ions). The negative ions that pass through a 2 mm diam skimmer are collinearly accelerated to 1 keV. Mass selection is achieved with a 1 m long beam-modulated time-of-flight mass spectrometer.[32] The mass-separated anions then enter the detection region where they are photodetached by a (pulsed) excimer-pumped dye laser in either of two locations: 60 cm upstream of the ion and electron detectors (the region labeled "A" in Fig. 2) or adjacent to the ion and electron detectors in the region labeled "B" in Fig. 2. For photodetachment of linear C_6^-, the dye laser output was doubled with a β-barium borate (BBO) crystal. The dyes used were Rhodamine 600 (300–310 nm), Rhodamine 590 perchlorate (287–300 nm), and Coumarin 540 (270–289 nm).

Three types of photodetachment experiments can be performed with this instrument. We can obtain threshold photodetachment spectra and "partially discriminated" photodetachment cross sections by photodetaching the anions at "A." Total photodetachment cross sections are obtained by photodetachment at "B," directly below the electron detector (marked with the ⊗ in Fig. 2). In all three experiments, the electron signal is normalized with respect to the ion current and laser power. Each mode of operation will now be described in more detail.

Threshold photodetachment spectra are obtained by adapting the zero electron kinetic energy (ZEKE) spectroscopy method developed by Müller-Dethlefs *et al.*[33] to negative ion photodetachment. In these experiments, C_6^- clusters are photodetached in region A. The ejected photoelectrons are extracted with a pulsed field of about 2 V/cm, which is applied 200 ns after the photodetachment laser pulse. This delay allows the higher energy electrons to separate spatially from the threshold electrons that have nearly zero kinetic energy. Once the field is applied, the energetic electrons with significant velocity perpendicular to the ion beam direction are prevented from reaching the detector by a series of apertures between the extraction region and electron detector. Threshold electrons and higher energy electrons scattered along the ion beam axis pass through a 60 cm long Einzel lens and are then deflected into the electron detector with a weak field. While these higher energy electrons cannot be discriminated against by the apertures, they emerge from the extraction region with different kinetic energies than the threshold electrons, due to the spatial separation along the beam axis that occurs prior to applying the extraction pulse. The higher energy electrons can then be discriminated against with a gated detection scheme, in which only those electrons arriving at the detector within a 35 ns window are counted. This combination of spatial and temporal discrimination yields an electron energy resolution of 3 cm^{-1}. The resulting peak for an ideal atomic system (one which undergoes *s*-wave detachment near threshold[30,34]) is shown in Fig. 3(a).

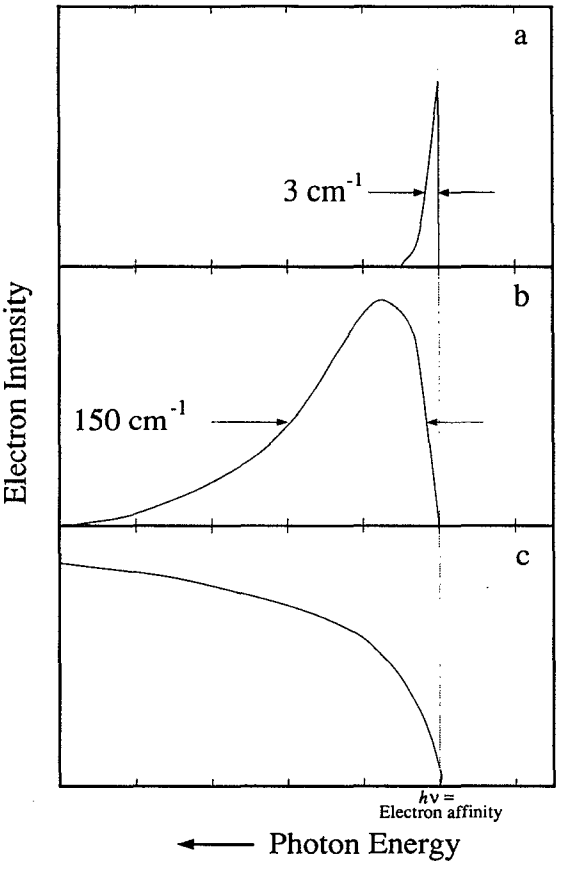

FIG. 3. Idealized appearance photodetachment signal (in the absence of autodetachment) for the three modes of operation of the instrument: (a) threshold photodetachment spectrum, (b) "partially discriminated" cross section, and (c) total photodetachment cross section.

If the C_6^- clusters are photodetached at A and the extraction pulse is applied with no delay, one obtains a "partially discriminated" photodetachment cross section scan. The electron extraction field immediately accelerates all of the photoelectrons toward the electron detector. However, those photoelectrons produced with a significant perpendicular velocity component are still spatially discriminated against by the apertures *en route* to the electron detector. This is therefore a variation on the "steradiancy detector" described many years ago by Spohr *et al.*[35] and Baer *et al.*[36] The result is an asymmetric peak which is about 150 cm^{-1} wide [Fig. 3(b)]; the collection efficiency drops off dramatically for electrons produced with more than 150 cm^{-1} kinetic energy. Hence, scans performed in this mode of operation are referred to as "partially discriminated" photodetachment cross section scans.

Finally, to measure the total photodetachment cross section, the clusters are photodetached via the second set of laser windows at region B, which lies just below the electron detector. All of the photoelectrons are collected with a 10 V/cm extraction field. The resulting cross section for an ideal atomic system (*s*-wave photodetachment) will resemble the spectrum in Fig. 3(c).

This article is copyrighted as indicated in the article. Reuse of AIP content is subject to the terms at: http://scitation.aip.org/termsconditions. Downloaded to IP: 129.174.21.5 On: Wed, 24 Dec 2014 14:15:05

If direct photodetachment is all that is occurring, there is little reason to perform anything other than threshold photodetachment spectroscopy with this instrument. However, electrons resulting from autodetachment processes will often have considerably more than 3 cm^{-1} kinetic energy and will therefore not be observed in a threshold photodetachment spectrum, so the instrument must be operated in one of the other two modes to study autodetachment. In the "partially discriminated" mode of operation, only relatively low energy electrons from autodetachment will be collected efficiently, while virtually all the photoelectrons produced by autodetachment will be collected in the total cross section mode. Differences in the intensity of autodetachment peaks obtained in these two modes can serve as a qualitative measure of the electron kinetic energy resulting from autodetachment.

In addition to the above experiments, photodetachment power studies and two-color, two-photon photodetachment scans are reported in this paper. These are done in order to ascertain the importance of single photon vs multiphoton detachment for the various peaks observed in the total photodetachment cross section. The photodetachment power studies entail counting electrons produced in region B as a function of laser pulse energy for a particular detachment wavelength. The electrons are counted for 5000–6000 laser shots at a given laser power and normalized to the collected ion current. In the two-color, two-photon scans, C_6^- is photodetached at "B" by copropagating, simultaneous laser pulses from the doubled dye laser and the second harmonic of a Nd:YAG laser (532 nm). The two laser pulses are made simultaneous with the aid of a photodiode. For these experiments, the dye laser fluence was 25 mJ/cm^2 (0.5 mJ/pulse) and the 532 nm fluence was 100 mJ/cm^2 (2 mJ/pulse). Any enhancement of the photodetachment signal by the YAG laser provides strong evidence for two-photon processes (see below).

III. RESULTS

Figures 4(a)–4(c) show the results of the three types of scans discussed in the experimental section for C_6^-. Figure 4(a) shows the threshold photodetachment spectrum, Fig. 4(b) shows the partially discriminated cross section, and Fig. 4(c) shows the total photodetachment cross secton.

The threshold photodetachment spectrum is dominated by peak A located at 296.65 nm. There are also three irregularly spaced peaks with approximately one-third the intensity of peak A at higher energies. The positions and relative energies of these peaks, labeled D, G, and I, are listed in Table I. A less intense peak is observed 29 cm^{-1} to the red of each of these peaks; these smaller peaks are labeled a, d, g, and i. All of the peaks in Fig. 4(a) are approximately 17 cm^{-1} wide [full width at half-maximum (FWHM)]. The rising baseline toward higher photon energies is due to background photoelectrons generated by stray photons impinging on various metal surfaces in the extraction region.

In the partially discriminated cross section scan [Fig. 4(b)], the direct photodetachment transitions [Eq. (1)] are

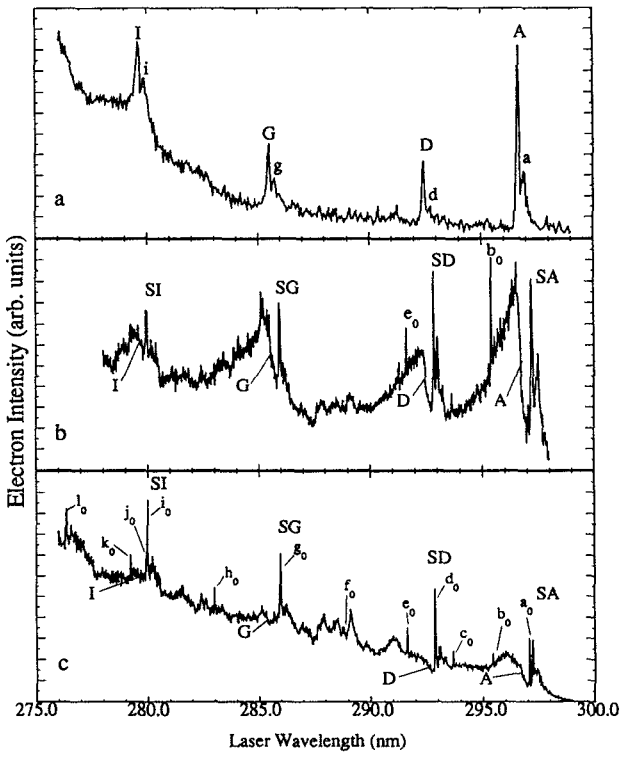

FIG. 4. (a) Threshold photodetachment spectrum of C_6^-. (b) Partially discriminated photodetachment cross section of C_6^-. (c) Total photodetachment cross section of C_6^-.

evident as distinct thresholds, which are at the same wavelengths as the peaks seen in the threshold photodetachment spectrum. These thresholds are also labeled A, D, G, and I. The electron signal near each threshold has the general appearance of the model spectrum in Fig. 3(b), rising sharply then decreasing gradually in intensity as the photon energy increases. In addition, a series of sharp peaks are observed which do not appear in Fig. 4(a). These are due to transitions to excited states of the anion followed, in most cases, by autodetachment [Eq. (2)]. Four manifolds of these peaks lie just to the red of the four direct detachment thresholds and are labeled SA, SD, SG, and SI in reference to the thresholds to which they correspond. There are also two fairly intense individual peaks (b_0 and e_0) that do not appear to correspond to direct photodetachment thresholds.

In the total photodetachment cross section scan [Fig. 4(c)] the direct detachment thresholds, again labeled A,

TABLE I. Peak positions, relative energies, and assignments for the threshold photodetachment spectrum of C_6^-.

Peak	Position (nm)	Relative energy (cm^{-1})	Assignment	Calculation (Matrin) (Ref. 20)
A	296.65	0	Origin[a]	...
D	292.41	489(10)	3_0^1	673
G	285.45	1322(10)	2_0^1	1759
I	279.56	2061(10)	1_0^1	2167

[a]This corresponds to an electron affinity of 4.180(0.001) eV.

This article is copyrighted as indicated in the article. Reuse of AIP content is subject to the terms at: http://scitation.aip.org/termsconditions. Downloaded to IP: 129.174.21.5 On: Wed, 24 Dec 2014 14:15:05

TABLE II. Peak positions, relative energies, and assignments (Sec. IV) for the total cross section spectrum of C_6^-. The calculated energies are based on an MP2/6-31G* calculation (Ref. 20) predicting the harmonic frequencies: $\nu_1=2167$, $\nu_2=1759$, $\nu_3=673$, $\nu_4=2009$, $\nu_5=1244$, $\nu_6=551$, $\nu_7=223$, $\nu_8=432$, and $\nu_9=108$.

Peak	Position (nm)	Relative energy (cm^{-1})	Assignment	Calculation (Ref. 20) (cm^{-1})
a_0	297.019	0	Origin	...
b_0	297.386	186(2)	9_0^2	216
c_0	293.622	390(2)	7_0^2	446
d_0	292.84	480(2)	3_0^1	673
e_0	291.60	626(2)	8_0^2	862
f_0	288.77	962(3)	3_0^2	1346
g_0	285.92	1307(5)	2_0^1	1759
h_0	282.95	1674(5)	5_0^2	2488
i_0	279.91	2058(5)	1_0^1	2167
j_0	279.87	2063(5)	$5_0^2 7_0^2$	2934
k_0	279.17	2153(5)	$5_0^2 3_0^1$	3161
l_0	276.28	2527(5)	$1_0^1 3_0^1$	2840
m_0	270.31	3327(5)	$1_0^1 2_0^1$	3926

D, G, and I, are considerably less distinct than in Fig. 4(b). On the other hand, the autodetachment peaks are more intense relative to the direct detachment thresholds. The most intense peaks in each of the four manifolds SA, SD, SG, and SI, are labeled a_0, d_0, g_0, and i_0. In addition, several sharp but less intense autodetachment peaks not observed in the partially discriminated scan appear in the total cross section scan; these are labeled b_0, c_0, etc. In both Figs. 4(b) and 4(c), the SA manifold does not dominate over the other sharp peak manifolds as peak A in Fig. 4(a) dominates over the rest of the peaks. However, the SD, SG, and SI manifolds in the total cross section scan have comparable intensities, while in the partially discriminated scan, they decrease in intensity toward the higher photon energies. The positions and relative energies of the labeled peaks are listed in the first three columns of Table II. Note that peak m_0 is not shown in Fig. 4(c), but it has approximately the same intensity as peak k_0. Also, there are several broad peaks in Fig. 4(c) which have not been assigned.

Figures 5(a) and 5(b) and 6(a) and 6(b) show expanded-scale, finer-step scans of the SA and SB manifolds, respectively. Figures 5(a) and 6(a) show the partially discriminated cross section, while Figs. 5(b) and 6(b) show the total cross section. These figures reveal that these manifolds consist of several peaks of 5–7 cm^{-1} FWHM, many of which are actually partially resolved doublets with a characteristic splitting of ~ 1.7 cm^{-1}. This splitting is most likely due to the contours of unresolved rotational transitions. The rotational constant for C_6^- is expected to be around 0.04 cm^{-1}, so individual rotational transitions cannot be observed at our current resolution (0.4 cm^{-1}). This splitting does not appear in peaks belonging to the higher energy SG and SI manifolds. Table III lists the peak positions and relative energies for Fig. 5(b). For those peaks which appear as doublets, the peak positions and relative energies refer to the center of the doublet.

The total cross section and partially discriminated

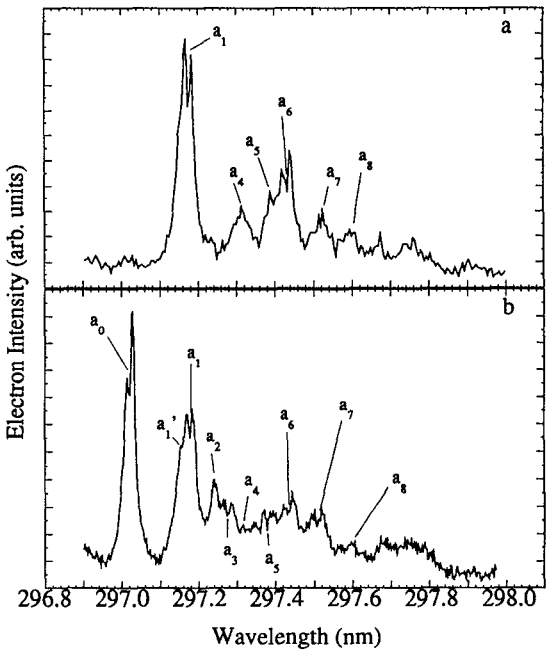

FIG. 5. (a) Expanded-scale, finer-step close up scan of the SA manifold taken in the partial discrimination mode. (b) Expanded-scale, finer-step close up scan of the SA manifold taken in the total cross section mode.

scans of the the SA manifold at 297 nm are very different. The most intense feature in Fig. 5(b) is the a_0 doublet at 297.019 nm. This is almost completely missing in the partially discriminated scan, and implies that the corresponding electrons are highly energetic. Note that the largest peak in the SA manifold in Fig. 4(b) is a_1, not a_0. The a_2 peak and the a_3 doublet in Fig. 5(b) are also virtually

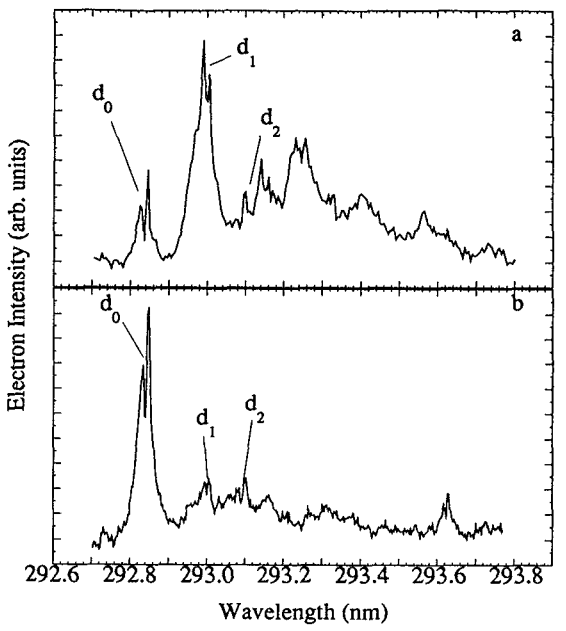

FIG. 6. (a) Expanded-scale, finer-step close up scan of the SD manifold taken in the partial discrimination mode. (b) Expanded-scale, finer-step close up scan of the SD manifold taken in the total cross section mode.

This article is copyrighted as indicated in the article. Reuse of AIP content is subject to the terms at: http://scitation.aip.org/termsconditions. Downloaded to IP: 129.174.21.5 On: Wed, 24 Dec 2014 14:15:05

TABLE III. Positions, relative energies, and proposed assignments (Sec. IV) for the peaks found within the SA manifold.

Peak	Position (nm)	Relative energy (cm^{-1})	Proposed assignment
a_0	297.019	0	Origin
a_1	297.179	−18.1(1)	9_1^1
a_2	297.241	−25.1(2)	7_1^1
a_3	297.277	−29.2(2)	S–O
a_4	297.317	−33.7(3)	9_2^2
a_5	297.380	−40.9(3)	$7_1^1 9_1^1$
a_6	297.439	−47.5(3)	9_1^1 *plus* S–O
a_7	297.509	−55.5(3)	$7_1^1 9_2^2$
a_8	297.582	−63.7(3)	9_2^2 *plus* S–O

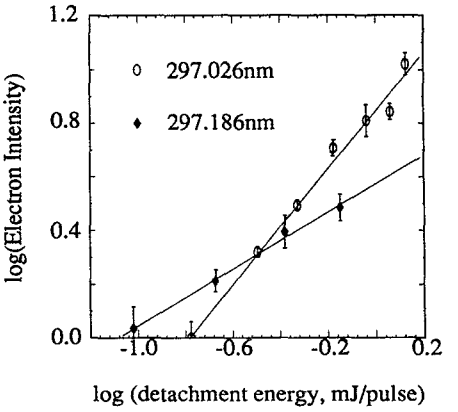

FIG. 8. Anion photodetachment as a function of detachment pulse energy for peaks a_0 and a_2 in the SA manifold.

absent in Fig. 5(a). The differences between Figs. 6(a) and 6(b) are not quite as dramatic. The most intense feature in the total cross section scan, the d_0 doublet at 292.84 nm, is much smaller relative to the other features in the partially discriminated scan.

Figures 7(a) and 7(b) show total cross section scans from 292–298 nm under two different ion source conditions. The He backing pressure in Fig. 7(a) is considerably higher, so the vibrational temperature in Fig. 7(a) should be lower than in Fig. 7(b). The data shows that the intensities of peaks a_0 and d_0 are largely unaffected by source conditions, but the features just to the red of each of these peaks are more intense in Fig. 7(b). These features are attributed to sequence bands from vibrationally excited C_6^- and are discussed in more detail below.

Figure 8 shows a log–log plot of the electron signal (in the total cross section mode) vs photodetachment laser pulse energy at 297.026 and 297.186 nm. These wavelengths correspond to the more intense peaks of the a_0 and a_1 doublets, respectively. The slope of the a_0 curve is approximately 1 while that of the a_1 curve is 0.5, indicating that the a_0 peak intensity depends linearly on laser pulse energy, while the a_1 intensity varies as the square root of the pulse energy. Hence, the a_1 transition appears more strongly saturated than the a_0 transition.

Figures 9(a) and 9(b) show the results of the two-color, two-photon scans performed on C_6^- for the SA manifold and part of the SD manifold, respectively. These scans are taken in the total photodetachment cross section mode and show the effect of an additional, simultaneous 532 nm pulse on the electron signal. The results are super-

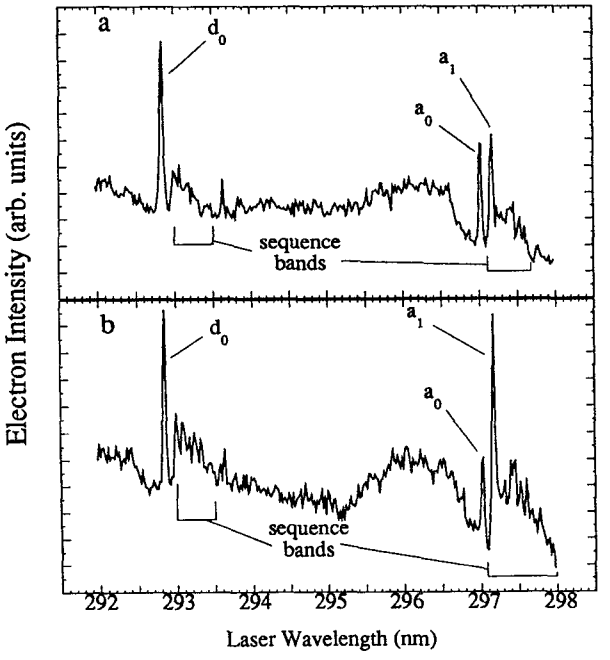

FIG. 7. (a) Total photodetachment cross section spectrum of C_6^- performed under normal ion conditions. (b) Total photodetachment cross section spectrum of C_6^- run with low carrier gas pressure.

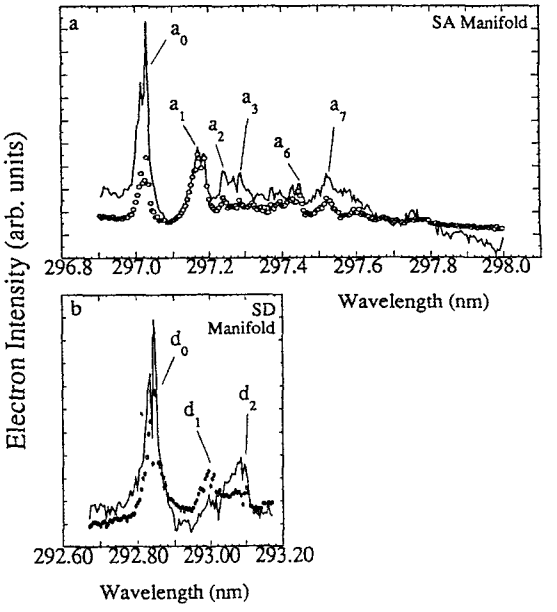

FIG. 9. (a) Two-photon, two-color scan (solid line) of SA manifold using tunable UV pulse (0.5 mJ/pulse) and simultaneous 2 mJ pulse at 532 nm. Scan with open circles is cross section at same UV pulse energy without 532 nm pulse. (b) Same as (a) for SD manifold.

This article is copyrighted as indicated in the article. Reuse of AIP content is subject to the terms at: http://scitation.aip.org/termsconditions. Downloaded to IP: 129.174.21.5 On: Wed, 24 Dec 2014 14:15:05

TABLE IV. Peak intensity changes between the one-photon and two-color, two-photon scans in the SA and SD manifolds.

Peak	Wavelength (nm)	Intensity(blue+green) / Intensity(blue only)
a_0	**297.019**	**3.0**
a_1	297.179	1.1
a_2	297.254	1.5
a_3	297.277	1.8
a_6	297.439	1
a_7	297.509	1.9
d_0	**292.84**	**1.6**
d_1	292.99	1
d_2	293.09	1.9

imposed on scans obtained under the same anion conditions and tunable dye laser power, but with no 532 nm pulse. Many of the peaks in these two regions exhibit a change in intensity with the addition of the 532 nm, but the most dramatic effect occurs for the 297.019 nm doublet (a_0); its intensity increases by a factor of 3 in the presence of both laser pulses. Almost no change in intensity was observed for the 297.179 nm doublet (a_1). The changes are less dramatic in Fig. 9(b); the intensity of the largest feature, the d_0 doublet, increases by a factor of 1.6 in the two-color scan. The relative intensities of the peaks in the one-color and two-color scans are given in Table IV.

IV. ANALYSIS AND DISCUSSION

A. Threshold photodetachment spectrum

1. Peak assignments

The C_6^- threshold photodetachment spectrum is dominated by peak A; peaks D, G, and I are about a factor of 3 smaller. We assign peak A to the origin of the $C_6 \leftarrow C_6^-$ direct photodetachment transition, while the higher energy peaks are assigned to transitions to vibrationally excited C_6 levels. The dominance of the origin transition indicates a small geometry change between the anion and neutral.

The doublet structure of the peaks of the threshold photodetachment spectrum strongly supports previous assignments of the C_6^- photoelectron spectrum in this energy range to a transition between linear C_6^- and linear C_6, as opposed to a transition between cyclic structures. The linear anion and neutral ground state term symbols are $^2\Pi_u$ (Refs. 21 and 22) and $^3\Sigma_g^-$,[16,19] respectively. The $^2\Pi_u$ state is split into two spin–orbit components with $\Omega=3/2$ (the lower of the two) and $\Omega=1/2$; if the splitting is small enough, both states will be significantly populated in the ion beam. Since the neutral $^3\Sigma_g^-$ state has no corresponding fine structure, each vibrational transition in the photodetachment spectrum should be a doublet, as we observe. The splitting in each doublet of 29 cm^{-1} is therefore the spin–orbit splitting C_6^-. For each doublet, the larger peak is from the $\Omega=3/2$ level, and the smaller from the spin–orbit excited $\Omega=1/2$ level. The intensity ratio gives an electronic temperature of approximately 40 K. For comparison, the spin–orbit splitting in the $^2\Pi_u$ state of C_5^- is 22 cm^{-1}.[17]

The electron affinity of linear C_6 is given by the energy at which peak A occurs, 4.180 ± 0.001 eV. For comparison, the best previous experimental value, from our C_6^- photoelectron spectrum, was 4.185 ± 0.006 eV.[15] *Ab initio* studies have also predicted electron affinities for linear C_6 in this range.[22,37]

We next consider the vibrational structure in our spectrum. In a photodetachment spectrum where the anion and neutral have different equilibrium geometries but the same overall symmetry, one expects progressions in totally symmetric vibrational modes of the neutral to dominate.[38] Linear C_6 has three totally symmetric modes (all symmetric stretches), and peaks D, G, and I are assigned to transitions to the fundamentals of the three modes. The resulting vibrational frequencies are $\nu_3=489\pm10$ (from peak D), $\nu_2=1322\pm10$ (peak G), and $\nu_1=2061\pm10$ cm^{-1} (peak I). Our ν_1 value is close to Martin's *ab initio* value of 2167 cm^{-1}.[20] However, our ν_2 and ν_3 frequencies are about 400 and 200 cm^{-1} lower, respectively, than the *ab initio* values. The experimental and calculated frequencies are summarized in Table I.

Note that cyclic C_6 in D_{3h} symmetry has only two totally symmetric modes; the *ab initio* study by Raghavachari and Binkley[39] predicts (scaled) frequencies of 1142 and 800 cm^{-1} for these modes. Thus, the number of transitions to vibrationally excited states in our spectrum is consistent with a linear $\leftarrow$ linear transition.

2. C_6 force constants

Since *ab initio* calculations overestimate the ν_2 and ν_3 frequencies, we have performed a simple, one-dimensional vibrational analysis on C_6 in order to determine the force constants that would reproduce our observed frequencies. The most general one-dimensional harmonic potential in symmetrized internal coordinates is

$$V=\tfrac{1}{2}(k_1s_1^2+k_2s_2^2+k_3s_3^2+k_4s_4^2+k_5s_5^2)+k^{\text{antisym}}s_4s_5 +k^{\text{sym},1}s_2s_3+k^{\text{sym},2}s_1s_3+k^{\text{sym},3}s_1s_2\,, \quad (3)$$

where s_1, s_2, and s_3 are symmetric combinations of the internal coordinates [$s_1=2^{-1/2}(\Delta r_a+\Delta r_e)$, $s_2=2^{-1/2}(\Delta r_b+\Delta r_d)$, and $s_3=\Delta r_c$] and s_4 and s_5 are antisymmetric combinations [$s_4=2^{-1/2}(\Delta r_a-\Delta r_e)$ and $s_4=2^{-1/2}(\Delta r_b-\Delta r_d)$]. The internal coordinates and all of the couplings between them as given by Eq. (3) are illustrated in Fig. 10. Because this is a six-body problem confined to one dimension, there is one translational degree of freedom and five vibrational degrees of freedom, corresponding to three symmetric stretches and two antisymmetric stretches. Therefore, in our attempts to reproduce our symmetric stretch frequencies, we will also generate two antisymmetric stretch frequencies.

As mentioned in the Introduction, Vala and co-workers confirmed that a 1952 cm^{-1} IR line absorbed by carbon clusters trapped in rare-gas matrices is due to a C_6 antisymmetric stretch (ν_4).[23] A frequency close to this has also been assigned to the ν_4 mode of C_6 in the *gas phase* in preliminary work done by Saykally and co-workers.[40] Years before, Thompson and co-workers[7] attributed a 1197

This article is copyrighted as indicated in the article. Reuse of AIP content is subject to the terms at: http://scitation.aip.org/termsconditions. Downloaded to IP: 129.174.21.5 On: Wed, 24 Dec 2014 14:15:05

cm^{-1} line to the lower frequency antisymmetric stretch (ν_5). Most of the assignments made in that work have since been reassigned, but this particular line has neither been disputed nor confirmed as of yet. Both of these frequencies are in reasonable agreement with calculations; Martin predicts the two antisymmetric stretches to be 1244 and 2009 cm^{-1} for the ν_5 and ν_4 modes, respectively.[20]

There are more force constants in Eq. (3) than there are frequencies to fit, and it is desirable to use the smallest possible number of parameters to fit the vibrational frequencies. First, we assume no coupling between the bonds (k^{antisym}, $k^{\text{sym},1-3}=0$) and $k_1=k_4$, $k_2=k_5$ giving the potential

$$2V=k_1(\Delta r_a^2+\Delta r_e^2)+k_2(\Delta r_b^2+\Delta r_d^2)+k_3\Delta r_c^2. \tag{4}$$

The symmetric stretch frequencies can be fit using Eq. (4), and the antisymmetric stretches obtained, 1112 and 1971 cm^{-1}, are close to the matrix values, but the resulting three force constants ($k_1=7.67$, $k_2=10.44$, $k_3=3.93$ mdyne/Å) are so different as to be unrealistic. For example, *ab initio* calculations on C_6 predict the central C–C bond to be slightly shorter than the others,[20] which is inconsistent with k_3 being the smallest force constant.

Alternatively, we can set all k_i's equal and assume coupling only between adjacent bonds ($k^{\text{sym},2}=0$, $k^{\text{sym},3}=k^{\text{antisym}}$) which gives the potential

$$V=\tfrac{1}{2}k_1(\Delta r_a^2+\ldots+\Delta r_e^2)+k^{\text{sym},3}(\Delta r_a\Delta r_b+\Delta r_d\Delta r_e)$$
$$+k^{\text{sym},1}(\Delta r_b\Delta r_c+\Delta r_c\Delta r_d). \tag{5}$$

Setting $k_1=7.28$, $k^{\text{sym},3}=-2.65$, and $k^{\text{sym},1}=1.23$ mdyne/Å reproduces the observed symmetric stretches, but also gives $\nu_4=2052$ cm^{-1}, which is slightly high, and $\nu_5=809$ cm^{-1}. While this model appears to be more realistic than the previous model, it produces an anomalously low ν_5 frequency. It is interesting to note that when typical carbon–carbon double bond force constants ($\sim$9.6 md/Å) are used in Eqs. (4) or (5), symmetric stretch frequencies very similar to the *ab initio* results are obtained.[18,20,41] As these are significantly higher than the experimental frequencies, the average bond order in C_6 appears to be somewhat less than two.

Further calculations including more coupling constants were performed to reproduce the 1197 cm^{-1} antisymmetric stretch frequency along with our observed symmetric stretch frequencies. However, even with a great deal of coupling, a very small center bond force constant was always required. Calculations performed with the restriction that the center bond remain comparable to the other bonds consistently produced a ν_5 frequency around 800 cm^{-1}. This raises the possibility that the ν_5 frequency, like the observed ν_2 and ν_3 frequencies, is much lower than predicted, and that the matrix assignment of the 1197 cm^{-1} line to the ν_5 mode in C_6 is incorrect. We note that a weak, unassigned line at 814 cm^{-1} was seen by Weltner and McLeod[6] in one of the first matrix isolation studies of carbon clusters, and that the ν_5 absorption is predicted to be considerably less intense than the ν_4 absorption.[20] While our force constant analysis cannot be regarded as definitive, it suggests that it would be worthwhile to perform the same isotopic substution studies on the 1197 and 814 cm^{-1} lines as were used to confirm the assignment of the 1957 cm^{-1} line to C_6, or to study these transitions in a rotationally resolved gas phase experiment.

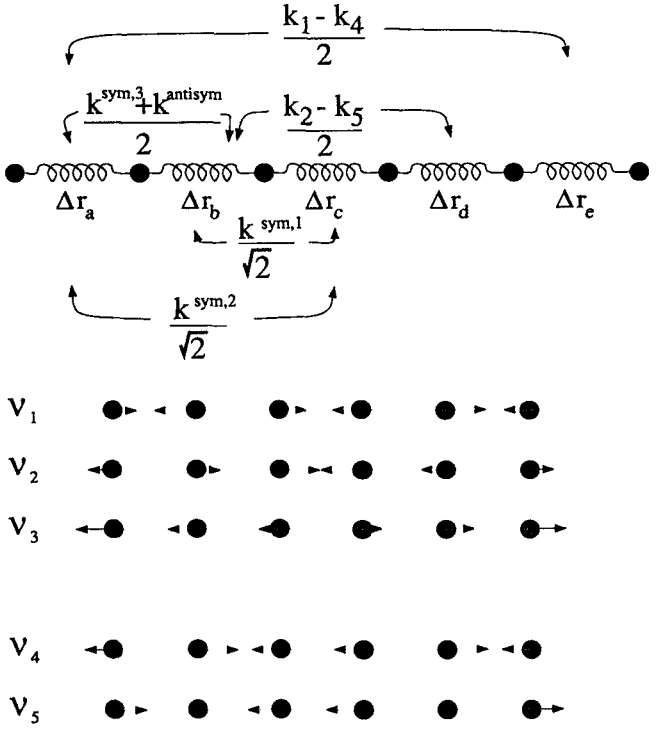

FIG. 10. Parameters for the one-dimensional vibrational calculation for C_6 and stretch normal modes for C_6. The modes ν_{1-3} are the symmetric stretches seen in the threshold photodetachment spectrum and $\nu_{4,5}$ are the antisymmetric stretches.

3. C_6^-/C_6 geometry change

The intensities of the peaks in the threshold spectrum are sensitive to the geometry change between the anion and neutral, and this change can be determined (approximately) by simulating the spectrum within the Franck–Condon approximation. The intensity of a transition between vibrational levels v'' and v' of the anion and neutral, respectively, is assumed proportional to the Franck–Condon factors (FCF)

$$I(v'\leftarrow v'')\propto|\langle\chi'_{\text{vib}}|\chi''_{\text{vib}}\rangle|^2. \tag{6}$$

The vibrational wave functions, χ_{vib}, are taken to be a product of three harmonic oscillator wave functions corresponding to the three symmetric stretches. Since the anion symmetric stretch frequencies are unknown, the anion potentials are taken to be identical to the neutral potentials (hence with the same frequencies), only displaced along the normal coordinate. This displacement is adjusted until the relative intensities in the simulation match those in the spectrum. Figure 11 shows the Franck–Condon simulation of the threshold photodetachment spectrum along with the actual spectrum. The three normal mode displacements in

This article is copyrighted as indicated in the article. Reuse of AIP content is subject to the terms at: http://scitation.aip.org/termsconditions. Downloaded to IP: 129.174.21.5 On: Wed, 24 Dec 2014 14:15:05

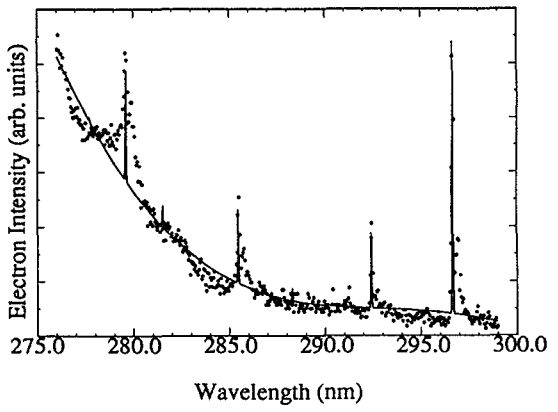

FIG. 11. Franck–Condon simulation of the threshold photodetachment spectrum of C_6^- using symmetric stretch normal coordinate displacements in text.

the simulation are $\Delta Q_1 = 0.033$, $\Delta Q_2 = 0.034$, and $\Delta Q_3 = 0.058$ (amu)$^{1/2}$ Å. These displacements reproduce the four peak intensities and do not result in appreciable transitions to overtone or combination levels of C_6.

In order to convert the normal mode displacement quantities to bond length changes, we first require a potential energy function in terms of bond length displacements and force constants which reproduces the experimental frequencies. We use the potential of Eq. (5) with the three force constants that gave the best fit to the symmetric stretch frequencies (listed previously).

To proceed further, we also require the sign of each normal mode displacement upon photodetachment. Unfortunately, the Franck–Condon factors depend only on the magnitudes of the displacements. There are eight possible combinations of signs in the three normal mode displacements, each yielding a different set of bond length changes. We can choose the most reasonable combination by comparing *ab initio* calculations of the anion[22,37] and neutral[18,37,41] geometries with the bond length changes from each combination. Calculations on C_6 predict the C–C bond lengths in the range of 1.29 Å which decrease slightly (by 0.02 Å) from the outermost to the central bond. In contrast, larger bond length variations are predicted in C_6^-; Adamowicz finds $r_a = 1.292$ (Ref. 22) (outermost bond—see Fig. 10), $r_b = 1.341$, and $r_c = 1.290$ Å, while Watts and Bartlett find $r_a = 1.258$, $r_b = 1.340$, and 1.237 Å.[37] The most consistent result is that r_b in the anion is significantly greater, about 0.050 Å, than in the neutral, a physically reasonable result since the $2\pi_u$ orbital from which photodetachment occurs is antibonding between the two carbon atoms.[19]

With our force constants, this result is reproduced only when all three normal coordinate displacements of the anion relative to the neutral are positive. (Figure 10 shows what is meant by positive for each normal mode.) This yields $\Delta r_a = 0.005$ (anion–neutral), $\Delta r_b = 0.057$, and $\Delta r_c = -0.057$ Å. Varying the ΔQ_n in the Franck–Condon simulation so that the simulated peak intensities have uncertainty falling within the experimental signal to noise changes the resultant bond length differences by about ± 0.005 Å. Although geometry changes are in better overall agreement with Bartlett's calculations than those of Adamowicz, they do result from several significant approximations and should be treated with appropriate caution. It should also be noted that the calculated geometries on which we base the sign of our normal coordinate displacement were determined in the same calculations that overestimated the ν_2 and ν_3 (and possibly ν_5) frequencies. However, geometries obtained in *ab initio* calculations are often more reliable than frequencies.

4. Comparison to the C_5^- threshold photodetachment spectrum

The overall appearance of the C_5^- and C_6^- spectra is qualitatively different. In the C_6^- spectrum, only transitions to excited symmetric stretch levels of C_6 are seen. These are all about one-third the intensity of the origin transition. In contrast, in the C_5^- spectrum, transitions to several bend levels in the neutral are evident and are nearly as intense as the transition to the C_5 ($\nu_2 = 1$) symmetric stretch level. However, the transitions to excited vibrational states of C_5 are at least a factor of 10 less intense than the origin. Transitions of this intensity would not be observable in the C_6^- spectrum because the signal to noise is such that the transitions would be obscured.

The higher intensity symmetric stretch transitions in the C_6^- spectrum imply larger bond length changes upon photodetachment. This is consistent with *ab initio* calculations of the C_5 and C_5^- geometries.[37] It therefore appears that the addition of an electron to the lowest unoccupied molecular orbital (LUMO) of C_5, the $2\pi_u$ orbital has less effect on the bond lengths than the addition of an electron to the (half filled) $2\pi_u$ LUMO in C_6.

B. Partially discriminated and total photodetachment cross section spectra

1. Peak assignments

Both the partially discriminated and total photodetachment cross section scans [Figs. 4(b) and 4(c)] feature fairly intense manifolds of sharp peaks ~43 cm^{-1} to the red of the direct detachment thresholds, which correspond to the ZEKE peaks seen in Fig. 4(a). These peaks are presumably due to transitions to a $(C_6^-)^*$ excited electronic state of the anion. Since these peaks so closely follow the direct detachment thresholds, they are assigned to the same vibrational transitions as the corresponding peaks in the threshold photodetachment spectrum. That is, the SA manifold marks the origin of the $(C_6^-)^* \leftarrow C_6^-$ transition, and the SD, SG, and SI manifolds are assigned to the 1_0^1, 2_0^1, and 3_0^1 transitions, respectively.

This assignment explains the observation of the 1_0^1, 2_0^1, and 3_0^1 transitions. The upper states in these transitions, namely the $v_1 = 1$, $v_2 = 1$, and $v_3 = 1$ levels of the excited $(C_6^-)^*$ state, can all decay to the $v = 0$ level of neutral C_6 by vibrational autodetachment. However, the SA manifold lies to the red of the detachment continuum. If this manifold includes the band origin, then the $v = 0$ level of the

This article is copyrighted as indicated in the article. Reuse of AIP content is subject to the terms at: http://scitation.aip.org/termsconditions. Downloaded to IP: 129.174.21.5 On: Wed, 24 Dec 2014 14:15:05

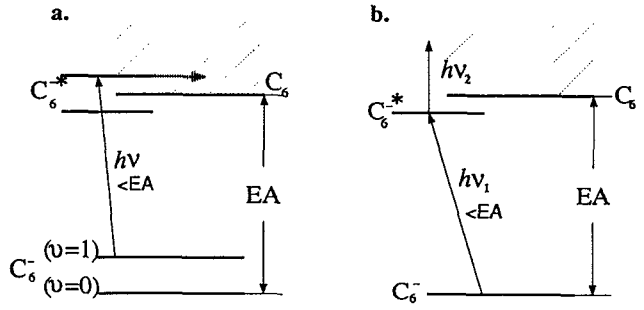

FIG. 12. Possible explanations for peaks in C_6^- photodetachment cross section at photon energies below detachment threshold [SA manifold, Fig. 4(c)]. (a) Peaks are hot bands from vibrationally excited C_6^-. (b) Peaks are from transitions to bound states which are photodetached by absorption of second photon.

$(C_6^-)^*$ excited state lies below the $v=0$ level of linear C_6. Thus, autodetachment from the $(C_6^-)^*$ $v=0$ level should not be energetically possible. The SA manifold therefore requires further discussion. We also need to explain the sharp peaks (b_0, e_0, etc.) that do not obviously correspond to peaks in the threshold photodetachment scan. In addition, there are congested clumps of peaks to the red of several of the strong transitions a_0, d_0, g_0, and i_0 in Figs. 4(b) and 4(c) which need to be explained.

SA manifold. All of the peaks in the SA manifold appear at a lower photon energy than the minimum needed to remove an electron from ground state C_6^- to form linear C_6. Two possible explanations for the appearance of this manifold in our photodetachment spectra are illustrated in Fig. 12.

Figure 12(a) shows that autodetachment can occur if peaks in the SA manifold are "hot band" transitions originating from vibrationally excited anion states, thereby requiring less energy to excite the C_6^- to a state lying above the detachment continuum. This hypothesis can be tested by varying the cluster source conditions to produce hotter ions, and observing how the intensities of the SA peaks vary relative to each other and to peaks in the higher-lying manifolds. The results [Figs. 7(a) and 7(b)] show that the intensities of peaks a_0 and d_0 are insensitive to source conditions, but the peaks just to the red of a_0 and d_0 are noticeably larger in the "hotter" scan [Fig. 7(b)]. Thus, the peaks to the red of peak a_0 in the photodetachment cross section arise from the situation in Fig. 12(a); they are sequence band transitions from vibrationally excited C_6^- to vibrationally excited levels of $(C_6^-)^*$ with sufficient energy to autodetach. However, the temperature studies suggest that peak a_0 at 297.019 nm is indeed the origin of the $(C_6^-)^* \leftarrow C_6^-$ transition, and its presence still requires explanation.

The most likely explanation for peak a_0 is that it results from a resonant two-photon transition where the first photon excites the ground anion electronic state to a *bound* excited anion state, and the second photon detaches the excited anion [Fig. 12(b)]. Resonant two-photon detachment through an intermediate state was first observed by Lineberger for C_2^- in 1972.[42] This explanation is consistent with several observations. In the first place, Figs. 5(a) and 5(b) show that peak a_0 is virtually absent in the partially discriminated scan, indicating that the electron kinetic energy associated with this peak is considerably higher than for the peaks to the red. This is just what would occur if peak a_0 results from two-photon absorption, whereas the other peaks are from one-photon absorption just above the detachment threshold followed by autodetachment.

Furthermore, the results in Fig. 8 indicate that the power dependence of peak a_0 differs from the other peaks in the SA manifold. The dependence of the intensity of peak a_0 on laser pulse energy is approximately linear, which at first glance suggests an unsaturated, one-photon process. However, the intensity of the adjacent peak, a_1, is proportional to the (pulse energy)$^{1/2}$, which suggests a *saturated* one-photon transition. Although not conclusive, the a_0 power dependence is consistent with a two-photon process in which the first step (between the two bound anion levels in our hypothesis) is strongly saturated.

Finally, we consider the two-color studies shown in Fig. 9. These were inspired by related work of Brauman and co-workers[43] on organic anions. Figure 9 shows a low power (0.5 mJ/pulse) total cross section scan with and without a simultaneous, more intense pulse (2 mJ/pulse) at 532 nm. The intensity of peak a_0 in the two-color scan is substantially increased, while that of peak a_1 is essentially unchanged. The 532 nm photon cannot detach ground state C_6^-, but can detach electronically excited $(C_6^-)^*$. Our results indicate that the $(C_6^-)^*$ state for peak a_0 is sufficiently long-lived so that it can be photodetached by a second photon, whereas the upper state for peak a_1 autodetaches too rapidly for the second photon to make any difference. This further supports the idea that peak a_0 is a transition to a level of $(C_6^-)^*$ which is bound with respect to autodetachment, while peak a_1 is a transition to a level above the detachment threshold.

All of this evidence shows that peak a_0 indeed is the vibrational origin of the $(C_6^-)^* \leftarrow C_6^-$ transition. Based on a comparison with the threshold photodetachment scan, the $v=0$ level of the excited anion state lies 43 cm^{-1} below the $v=0$ level of neutral C_6. This explains why the intensity of peak a_0 in the total cross section scan [Fig. 4(c)] is lower relative to the 1_0^1, 2_0^1, and 3_0^1 transitions than in the threshold photodetachment spectrum [Fig. 4(a)], where the origin transition is dominant. If, in the total cross section scan, peak a_0 is the only major peak that resulting from two-photon absorption, it is not surprising that its intensity is anomalously low.

Other manifolds. The assignment of the less intense but sharp features in the total cross section scan is not so obvious since there are no corresponding peaks in the neutral spectrum. While peak f_0 appears to be the 3_0^2 transition, the remaining peaks are most likely due to transitions to bend and antisymmetric stretch levels in the upper anion state; such transitions are allowed so long as the vibrational quantum number of the active mode changes by an even number.

Although no calculations for vibrational frequencies

This article is copyrighted as indicated in the article. Reuse of AIP content is subject to the terms at: http://scitation.aip.org/termsconditions. Downloaded to IP: 129.174.21.5 On: Wed, 24 Dec 2014 14:15:05

have been performed for the $(C_6^-)^*$ state, its symmetric stretch frequencies are essentially identical to those of neutral C_6. Assuming this holds for the nontotally symmetric vibrations as well, the less intense autodetachment peaks can be tentatively assigned by comparison with the corresponding frequencies from *ab initio* calculations performed on linear neutral C_6.[20] The assignments and comparison with *ab initio* values are shown in Table II. For example, peak b_0, 186 cm^{-1} to the blue of the origin, is assigned to the 9_0^2 transition; the ν_9 (π_u) mode is predicted to be the lowest frequency bend mode (216 cm^{-1} for two quanta).[20] Peak c_0, 390 cm^{-1} to the blue of the origin, is assigned to the 7_0^2 transition, in accordance with the calculated energy of 446 cm^{-1} for the $v_7=2$ level; the ν_7 mode, a π_g bend, is predicted to be the next-lowest frequency bending mode. Similarly, peak e_0, at 626 cm^{-1} to the blue of the origin, is assigned to the 8_0^2 transition and peak h_0, found at 1674 cm^{-1} to the blue of the origin, is assigned to the 5_0^2 transition. These latter two assignments are very tentative, since the deviation from the *ab initio* frequencies is significant, although the assigned ν_5 frequency is close to the ν_5 frequency determined in the one-dimensional calculation on C_6 using Eq. (5). The remaining sharp autodetachment peaks all appear at energies which are sums of the preceding bend and stretch frequencies, so they are assigned to combination transitions.

Sequence bands. Finally, we consider the sequence bands which are most evident to the red of peaks a_0 and d_0; see Figs. 5 and 6. The temperature studies (Fig. 7) show that most of these are transitions from vibrationally excited C_6^- in its $^2\Pi_u$ state to excited vibrational levels of the $(C_6^-)^*$ state. The assignment of these features is not straightforward; several of the peaks are only partially resolved, particularly in Fig. 5(b). However, there is a pattern to the peak spacings, with intervals of 18, 23, and 29 cm^{-1} appearing several times. In addition, the assignment is aided by comparing differences in peak intensities in the partially discriminated and total cross section scans, which are sensitive to the energy of the ejected electron, and the enhancement of peak intensities in the two-photon, two-color scan (Fig. 9), which is sensitive to the lifetime of the upper state with respect to autodetachment. Sets of peaks for which the intensities vary in the same way are most likely due to a common (or similar) upper state. Also, any two peaks split by 1.7 cm^{-1} are assigned to the same vibronic transition; as discussed above, this splitting is probably due to rotational contours in which individual rotational transitions are not resolved.

Peaks a_0, a_2, and a_3 appear in the total cross section scan but are missing in the partially discriminated scan. Peaks a_0 and a_3 are both doublets split by 1.7 cm^{-1}. They are separated by 29 cm^{-1}, which is the previously determined spin–orbit interval in the $^2\Pi_u$ ground state of C_6^-, and are both significantly enhanced in the two-color, two-photon experiment. Thus, we assign a_0 to the 0_0^0 transition originating from the $^2\Pi_{3/2}$ level of C_6^-, and peak a_3 to the same transition originating from the spin–orbit excited $^2\Pi_{1/2}$ level. This assignment implies that the spin–orbit splitting in the $(C_6^-)^*$ is negligible, a point which will be addressed later, and that the upper state of peak a_3, like that of peak a_0, is bound with respect to autodetachment. Peak a_2 is discussed below.

Peak a_1, 18 cm^{-1} to the red of peak a_0, is the second most intense feature in Fig. 5(b) and the most intense feature in Fig. 5(a). The significant intensity of this peak and its strong temperature dependence suggest it originates from the lowest excited vibrational level of C_6^{-1}, which, based on *ab initio* calculations on neutral C_6, should be the $v_9=1$ bending level. We therefore assign peak a_1 to the 9_1^1 sequence band. Our previous assignment of peak b_0 to the 9_0^2 transition, yields 93 cm^{-1} for the ν_9 frequency in the $(C_6^-)^*$ state, so the assignment of peak a_1 yields a ν_9 frequency of 111 cm^{-1} for the C_6^- ground state. With this assignment, the broad a_4 peak in Fig. 5(a), which is approximately 16 cm^{-1} to the red of the a_1 doublet, is assigned to the 9_2^2 transition. The assignment of these peaks to transitions involving the ν_9 mode is consistent with the observation of peak a_1 with high intensity in the partially discriminated scans [Figs. 4(b) and 5(a)]. The decay of the $v_9=1$ level of $(C_6^-)^*$ by vibrational autodetachment will result in a photoelectron with only 50 cm^{-1} of kinetic energy [obtained by subtracting 43 cm^{-1}, the amount by which the vibrationless $(C_6^-)^*$ state is bound, from 93 cm^{-1}, the $v_9=1$ vibrational energy in the $(C_6^-)^*$ state], and this will be collected efficiently in the partially discriminated mode of operation.

Peak a_6 is 29 cm^{-1} to the red of peak a_1, the same interval between peaks a_3 and a_0, so we assign it to the 9_1^1 transition from the spin–orbit excited $^2\Pi_{1/2}$ level of C_6^-. The small peak a_8, 16 cm^{-1} to the red of peak a_6, is then assigned to the 9_2^2 transition from the same spin–orbit level. The relative intensities of peak a_6 and a_1 are similar in Figs. 5(a) and 5(b), lending further support to our assignment.

Peak a_2 is 25 cm^{-1} to the red of peak a_0, and peak a_5 is 23 cm^{-1} to the red of peak a_1. It is reasonable to assign peak a_2 to the 7_1^1 sequence band transition, since the ν_7 bending mode should be the second lowest frequency vibration in C_6^-. Our previous assignment of peak c_0 to the 7_0^2 transition gives $\nu_7=195$ cm^{-1} in the $(C_6^-)^*$ state, so assigning peak a_2 to the 7_1^1 transition yields $\nu_7=220$ cm^{-1} in the anion ground state. Peak a_5 is then the $7_1^1 9_1^1$ combination transition. We assign peak a_7, 15 cm^{-1} to the red of peak a_5, to the $7_1^1 9_2^2$ transition.

Note that peak a_2 is prominent in the total cross section scan but not in the partially discriminated scan, while peaks a_5 and a_7 are clearly visible in the partially discriminated scan. This indicates that the ejected photoelectrons are less energetic for peaks a_5 and a_7. Vibrational autodetachment from the $v_7=1$ level of $(C_6^-)^*$ (the presumed upper level for peak a_2) to the C_6 ground state results in a photoelectron with 152 cm^{-1} of kinetic energy. On the other hand, both the $(v_7=1, v_9=1)$ and $(v_7=1, v_9=2)$ levels of the $(C_6^-)^*$ can autodetach via a $\Delta v_9=-1$ transition, yielding 50 cm^{-1} electrons in both cases. Hence, the observed intensities of the three peaks in Figs. 5(a) and 5(b) is qualitatively consistent with our assignment.

Table III gives a summary of all of the sequence band assignments. Several of these assignments, particularly

This article is copyrighted as indicated in the article. Reuse of AIP content is subject to the terms at: http://scitation.aip.org/termsconditions. Downloaded to IP: 129.174.21.5 On: Wed, 24 Dec 2014 14:15:05

those involving the ν_7 mode, must be regarded as somewhat tentative. Also, we have not considered complications from Renner–Teller activity in the excited bending modes for the anion $^2\Pi_u$ ground state. A possible contribution from this effect is the additional feature a_1' in Fig. 5(b). The a_1'–a_1 feature is noticeably broader than the a_0 doublet and in fact appears to be two superimposed doublets separated by 2 cm^{-1}. This could directly reflect the Renner–Teller splitting in the ν_9 mode of the anion.

2. Autodetachment mechanism and autodetaching state lifetimes

The mechanisms for autodetachment of negative ions and the analogous process, autoionization of neutrals, have been extensively discussed in the literature.[44–47] For our $(C_6^-)^*$ state, where the $v=0$ level is bound but all vibrationally excited levels lie above the detachment threshold, vibrational autodetachment is the most likely mechanism. In this case, autodetachment occurs by a breakdown of the Born–Oppenheimer approximation. The electronic wave functions for the excited anion state and neutral are coupled via the nuclear vibrational kinetic energy operator $\hat{T}_{\text{vib}}$, and autodetachment occurs when one (or more) quanta of vibrational energy in the anion is converted to electronic energy, resulting in the ejection of an electron.

More specifically, the vibrational autodetachment rate from the initial state with $v_k=n$ is given by[45]

$$\text{rate} \propto \frac{2\pi}{\hbar} |\langle \Psi_f | \hat{T}_{\text{vib}} | \Psi_i \rangle|^2 \rho, \tag{7}$$

where $\Psi_i = \psi_{el,i}\chi_{\text{vib},i}$ and $\Psi_f = \psi_{el,f}\chi_{\text{vib},f}$ are the vibronic wave functions for the excited anion and (neutral + electron), respectively, and ρ is the density of states for the (neutral + electron) continuum. The matrix element in Eq. (7) is given by

$$\langle \Psi_f | \hat{T}_{\text{vib}} | \Psi_i \rangle = -\frac{\hbar^2}{\mu} \left\langle \chi_{\text{vib},f} \left| \left\langle \psi_{el,f} \left| \frac{d}{dQ_k} \psi_{el,i} \right. \right\rangle \frac{d}{dQ_k} \chi_{\text{vib},i} \right. \right\rangle. \tag{8}$$

If the inner integral over electronic coordinates is assumed constant, and $\chi_{\text{vib},i}$ and $\chi_{\text{vib},f}$ are taken to be harmonic oscillator wave functions, then only $\Delta v_k=-1$ transitions are allowed. This propensity rule was used in the previous section in determining the electron kinetic energies from autodetachment out of excited vibrational levels of the $(C_6^-)^*$ state, although for several of these states, $\Delta v_k=-1$ transitions are the only possible transitions.

The lifetimes of autodetaching states are best determined by measuring spectral linewidths. Unfortunately, we cannot resolve individual rovibronic transitions in these spectra. We can estimate limits on the lifetimes, however, based on a few observations.

We first consider the transitions to excited symmetric stretch levels of the $(C_6^-)^*$ state. Peak d_0, the 3_0^1 transition, shows the characteristic 1.7 cm^{-1} splitting attributed to rotational contours. This splitting is not resolved for peaks $g_0(2_0^1)$ and i_0 (1_0^1). If this lack of structure is due to lifetime broadening, then the autodetachment lifetimes of the $v_1=1$ and $v_2=1$ levels are less than 1 ps, while that of the $v_3=1$ level is longer (actually much longer, as shown below). However, in the absence of full rotational resolution, we cannot rule out spectral congestion as the source of the broadening of the 2_0^1 and 1_0^1 transitions.

We obtain another, more interesting, measure of autodetachment lifetimes from the two-photon, two-color scans (see Fig. 9 and Table IV). If the intensity of a peak is enhanced in those scans, then the state accessed by the ultraviolet photon is either bound and has a fluorescence lifetime comparable to or greater than the laser pulse width (peaks a_0, a_3), or it is quasibound with its autodetachment lifetime comparable to or greater than its fluorescence lifetime as well as the laser pulse width (predissociation should not be energetically allowed). In the latter case, the autodetachment lifetime must be in the nanosecond range. We find that peaks d_0, d_2, a_2, and a_7 are noticeably enhanced; the first two are the two spin–orbit components of the 3_0^1 transition, and the second two are sequence band transitions in which the upper state can autodetach only by a $\Delta v_7=-1$ transition. Hence, the lifetimes for autodetachment through the ν_7 and ν_3 modes are at least several nanoseconds. On the other hand, the peaks in which the upper state can autodetach via a $\Delta v_9=-1$ transition (a_1,a_6) show no enhancement, but the 1.7 cm^{-1} splitting is still resolvable. So long as the fluorescence lifetime is similar for the $v_3=1$, $v_7=1$, and $v_9=1$ levels of the $(C_6)^*$ state, this result means that the autodetachment lifetime of a state which can autodetach by a $\Delta v_9=-1$ transition is greater than 2 ps, but is significantly shorter than the autodetachment lifetime of a state that must autodetach by a $\Delta v_7=-1$ or $\Delta v_3=-1$ transition.

This mode-specific effect is striking and deserves further discussion. The density of states factor ρ in Eq. (2), which is proportional to the (electron kinetic energy)$^{1/2}$, is smaller for a $\Delta v_9=-1$ transition than for a $\Delta v_7=-1$ or $\Delta v_3=-1$ transition. Thus, the matrix element $\langle \Psi_f | \hat{T}_{\text{vib}} | \Psi_i \rangle$ must be substantially larger for a $\Delta v_9=-1$ transition. This will be the case if the inner integral in Eq. (8) over the electron coordinates, $\langle \psi_{el,f} | d(\psi_{el,i})/dQ_k \rangle$, is larger for the ν_9 mode than for the other two modes, which, in turn, requires that the derivative of the $(C_6^-)^*$ electronic wave function with respect to Q_9 is large. While the nature of $\psi_{el,i}$ is uncertain (see next section), the ν_9 mode is a low-frequency, large amplitude bending mode. One might therefore expect the electronic wave function to be quite different at the classical turning points for the $v_9=1$ level than at the equilibrium geometry, while for a higher frequency, lower amplitude mode, this effect would not be so pronounced. A more quantitative treatment along the lines developed by Simons[48] would be extremely useful in understanding the autodetachment phenomena observed here.

3. Nature of the excited anion state

The molecular orbital configurations of the C_6^- and C_6 ground states are

$$C_6^-(^2\Pi_u): \ldots(1\pi_u)^4(6\sigma_u)^2(7\sigma_g)^2(1\pi_g)^4(2\pi_u)^3,$$

This article is copyrighted as indicated in the article. Reuse of AIP content is subject to the terms at: http://scitation.aip.org/termsconditions. Downloaded to IP: 129.174.21.5 On: Wed, 24 Dec 2014 14:15:05

$$C_6(^3\Sigma_g^-): \ldots(1\pi_u)^4(6\sigma_u)^2(7\sigma_g)^2(1\pi_g)^4(2\pi_u)^2.$$

The $(C_6^-)^*$ excited electronic state can result from excitation from one of the lower-lying orbitals to the partially filled $2\pi_u$ orbital, or by promotion of a $2\pi_u$ electron to a higher-lying, empty orbital. The correspondence between vibrational features in the C_6^- threshold photodetachment and autodetachment spectra indicates that $(C_6^-)^*$ and neutral C_6 have similar nuclear geometries. This is consistent with the second type of excited state, with the added proviso that the $2\pi_u$ electron is promoted to a nonbonding orbital.

The nature of this orbital is of considerable interest. Autodetachment has previously been observed from two types of excited electronic states in molecular negative ions: valence states, in which the highest occupied molecular orbital is a "conventional" molecular orbital, and electrostatically bound states, in which the outermost electron is in a very diffuse orbital and is bound to the neutral core via long-range electrostatic attraction. An example of the former is C_2^-,[26] while examples of the latter include dipole-bound states, such as in CH_2CHO^- (Ref. 49) and CH_2CN^-,[50] and the "image charge-bound" states proposed to explain autodetachment in Au_6^-.[51]

The $(C_6^-)^*$ state does not appear to be a clear-cut example of either type of excited state. The similarity between the $(C_6^-)^*$ and C_6 nuclear geometries is what would be expected if $(C_6^-)^*$ were electrostatically bound, consisting of an electron weakly interacting with the neutral C_6 core. The apparent absence of spin–orbit splitting in the $(C_6^-)^*$ state is consistent with such a picture. In addition, the small binding energy (43 cm^{-1}) is characteristic of such a state. While $(C_6^-)^*$ obviously cannot be a dipole-bound state, an "image charge-bound" state (or, perhaps more accurately, a "polarization-bound" state) cannot be ruled out. These states have not been nearly as thoroughly investigated as dipole-bound states,[52] but such a state might result if the polarizability of the π-electron network in the C_6 core were sufficiently high. However, we do not observe autodetachment near the detachment threshold for C_4^- or C_8^-. If $(C_6^-)^*$ is an electrostatically bound state, it appears to be a special case among carbon cluster anions.

The $(C_6^-)^*$ state could also result from excitation to an excited valence orbital. While bound valence-excited states for anions are rare, C_6^- is an open-shelled molecule with a high electron binding energy and has several low-lying, unfilled π orbitals, so the existence of such a state would not be surprising. This is supported in the work by Adamowicz,[22] who calculated vertical excitation energies to eight bound exited anion states of C_6^- which involve only valence orbitals. In particular, an optically accessible $^2\Pi_g$ state is predicted to lie just below the detachment threshold; this state results from excitation of a $2\pi_u$ electron to a low-lying π_g^* orbital.

If this state is actually the observed $(C_6^-)^*$ state, then the π_g^* orbital must be completely nonbonding, so that the excited anion state geometry is similar to that of the neutral. In addition, we observe the same spin–orbit splitting (29 cm^{-1}) in the autodetachment spectrum as in the threshold photodetachment spectrum, indicating negligible spin–orbit interaction in the $(C_6^-)^*$ state (there is none in the $C_6\,^3\Sigma_g^-$ state). Thus, if the $(C_6^-)^*$ state is indeed a $^2\Pi_g$ state, it must be very good example of Hund's case (b) coupling. Whether these constraints on the π_g^* orbital eliminate it from consideration remain to be seen. Of course, the upper state could also be a Σ_g state resulting from excitation of a $2\pi_u$ electron to a σ_g orbital; this would be consistent with the observed spin–orbit structure. No such states have been predicted near the detachment threshold, however.

The above discussion shows that the classification of the $(C_6^-)^*$ state as an electrostatically bound or valence state is difficult. Both labels have their attractions and their pitfalls. In our view, the evidence points more towards a valence state at this point. More insight should result from rotationally resolved resonant two-photon detachment experiments via the bound $(C_6^-)^*$ levels. In addition, *ab initio* studies of the geometries, and not just the vertical excitation energies, of the C_6^- excited states would be extremely useful.

V. CONCLUSION

We have performed two types of photodetachment spectroscopy on C_6^-: threshold photodetachment (ZEKE) spectroscopy, which maps out transitions between C_6^- and C_6, and autodetachment spectroscopy, which reveals an excited state of C_6^- 43 cm^{-1} below the detachment threshold.

The vibrational and spin–orbit structure in the threshold photodetachment spectrum is consistent with a transition between linear C_6^- and C_6. The spectrum yields the three symmetric stretch frequencies of C_6, as well as the spin–orbit splitting in the C_6^- ground $^2\Pi_u$ state. Two of our three frequencies are noticeably lower than previous *ab initio* results. From these frequencies and the peak intensities, we have used a simple force field model to derive force constants and bond displacements between the anion and neutral. In order to match the experimental frequencies, the force constants between adjacent carbon atoms had to be dropped significantly from typical carbon–carbon double bond force constants.

The autodetachment results show that the $(C_6^-)^*$ state is very similar to the neutral linear C_6 state. We observe transitions to the origin and excited symmetric stretch levels of the $(C_6^-)^*$ state which are all shifted 43 cm^{-1} to the red of corresponding features of the threshold photodetachment spectrum. Since the $v=0$ level of the $(C_6^-)^*$ state is bound with respect to the linear neutral, the electron signal we observe from this state results from a two-photon process. We also observe weaker transitions to excited bending and antisymmetric stretch levels of the $(C_6^-)^*$ state, as well as sequence bands originating from vibrationally excited levels of the C_6^- ground state. Two-color, two-photon studies indicate differing autodetachment lifetimes for the various vibrational levels of the $(C_6^-)^*$ state; autodetachment by a $\Delta v_9 = -1$ transition (π_u bend) is noticeably faster than $\Delta v_3 = -1$ (symmetric stretch) or Δv_7

This article is copyrighted as indicated in the article. Reuse of AIP content is subject to the terms at: http://scitation.aip.org/termsconditions. Downloaded to IP: 129.174.21.5 On: Wed, 24 Dec 2014 14:15:05

$=-1$ (π_g bend) transitions. We lean towards assigning the $(C_6^-)^*$ state as a valence-excited state rather than an electrostatically bound state. *Ab initio* calculations predict a valence-excited $^2\Pi_g$ state near the detachment threshold, but the $(C_6^-)^*$ state does exhibit several properties one would expect in an electrostatically bound state.

Finally, we point out that while this experiment shows no evidence for a cyclic C_6 state close in energy to the linear C_6 state, the existence of such a state cannot be ruled out. Any transitions from a linear anion to cyclic neutral will be spread out over a large energy range due to the substantial geometry change and therefore would be difficult to observe in this experiment. Although our earlier C_6^- photoelectron spectrum showed a low energy "tail" which may have come from cyclic C_6^-, which is predicted to lie about 1 eV above the linear anion geometry, no such tail was seen in the threshold photodetachment spectrum. This may indicate less cyclic C_6^- under the beam source operating conditions used here. In any case, if there is a cyclic C_6 state lower in energy than linear C_6, then the levels of the excited $(C_6^-)^*$ state which are bound with respect to linear C_6 should be able to autodetach to cyclic C_6. It may be possible to determine if this is occurring by measuring the C_6^- photoelectron spectrum at the photon energy corresponding to peak a_0. This experiment will be carried out shortly in our laboratory.

ACKNOWLEDGMENT

This research is supported by the National Science Foundation under Grant No. CHE-8857636.

[1] J. B. Edwards, *Combustion, Formation, and Emission of Trace Species* (Ann Arbor Science, Ann Arbor, 1974); J. R. Heath, S. C. O'Brien, R. F. Curl, H. W. Kroto, and R. E. Smalley, Comments Condensed Matter Phys. **13**, 119 (1987); H. W. Kroto and K. McKay, Nature **331**, 328 (1988).

[2] A. E. Douglas, Nature **269**, 130 (1979); R. F. Knake, *ibid.* **269**, 132 (1979); H. W. Kroto, J. R. Heath, S. C. O'Brien, R. F. Curl, and R. E. Smalley, Astrophys. J. **314**, 352 (1987); K. H. Hinkle, J. J. Keady, and P. F. Bernath, Science **241**, 1319 (1988).

[3] W. Weltner, Jr. and R. J. Van Zee, Chem. Rev. **89**, 1713 (1987).

[4] K. P. Huber and G. Herzberg, *Molecular Spectra and Molecular Structure IV: Constants of Diatomic Molecules* (Van Nostrand Reinhold, New York, 1979), Appendix IX and references therein.

[5] Representative references include W. Huggins, Proc. R. Soc. London **33**, 1 (1882); D. A. Ramsay, Adv. Spectrosc. **1**, 1 (1959); G. Herzberg, Astrophys. J. **96**, 314 (1949); L. Gausset, G. Herzberg, A. Lagerquist, and B. Rosen, Discuss. Faraday Soc. **35**, 113 (1965); K. Matsumura, H. Kanamori, K. Kawaguchi, and E. Hirota, J. Chem. Phys. **89**, 3491 (1988); E. A. Rohlfing, *ibid.* **91**, 4531 (1989).

[6] W. Weltner, Jr., P. N. Walsh, and C. L. Angell, J. Chem. Phys. **40**, 1299 (1964); **40**, 1305 (1964); **45**, 3096 (1966).

[7] K. R. Thompson, R. L. DeKock, and W. Weltner, Jr., J. Am. Chem. Soc. **93**, 4688 (1971).

[8] W. R. M. Graham, K. I. Dismuke, and W. Weltner, Jr., Astrophys. J. **204**, 301 (1976); W. Krätschmer, N. Sorg, and D. R. Huffman, Surf. Sci. **156**, 814 (1985); M. Vala, T. M. Chandrasekhar, J. Szczepanski, R. J. Van Zee, and W. Weltner, Jr., J. Chem. Phys. **90**, 595 (1989).

[9] S. Yang, K. J. Taylor, M. J. Craycraft, J. Conceicao, C. L. Pettiette, O. Cheshnovsky, and R. E. Smalley, Chem. Phys. Lett. **144**, 431 (1988).

[10] C_3: C. A. Schmuttenmaer, R. C. Cohen, N. Pugliano, J. R. Heath *et al.*, Science **249**, 897 (1990); C_4: J. R. Heath and R. J. Saykally, J. Chem. Phys. **94**, 3271 (1990); C_5: J. R. Heath, A. L. Cooksy, M. H. W. Grubele, C. A. Schmuttenmaer, and R. J. Saykally, Science **244**, 564 (1989); C_7: J. R. Heath, A. Van Orden, E. Kuo, and R. J. Saykally, Chem. Phys Lett. **182**, 17 (1991); J. R. Heath and R. J. Saykally, J. Chem. Phys. **94**, 1724 (1991); J. R. Heath, R. a. Sheeks, A. L. Cooksy, and R. J. Saykally, Science **249**, 895 (1990); C_9: J. R. Heath and R. J. Saykally, J. Chem. Phys. **93**, 8392 (1990).

[11] H. Sasada, T. Amano, C. Jarman, and P. F. Bernath, J. Chem. Phys. **94**, 2401 (1991); N. Moazzen-Ahmati, A. R. McKellar, and T. Amano, *ibid.* **91**, 2140 (1989).

[12] P. F. Bernath, K. H. Hinkle, and J. J. Keady, Science **244**, 562 (1989).

[13] K. M. Ervin and W. C. Lineberger, J. Phys. Chem. **95**, 1167 (1991).

[14] M. Polak, M. Gilles, and W. C. Lineberger (to be published).

[15] D. W. Arnold, S. E. Bradforth, T. N. Kitsopoulos, and D. M. Neumark, J. Chem. Phys. **95**, 8753 (1991).

[16] K. S. Pitzer and E. Clementi, J. Am. Chem. Soc. **81**, 4477 (1959).

[17] T. N. Kitsopoulos, C. J. Chick, Y. Zhao, and D. M. Neumark, J. Chem. Phys. **95**, 5479 (1991).

[18] K. Raghavachari, R. A. Whiteside, and J. A. Pople, J. Chem. Phys. **85**, 6623 (1986).

[19] V. Parasuk and J. Almölf, J. Chem. Phys. **91**, 1137 (1989).

[20] J. M. L. Martin, J. P. François, and R. Gijbels, J. Chem. Phys. **93**, 8850 (1990); J. Comput. Chem. **12**, 52 (1991). The listed calculations were performed on the MP2/6-31G* level.

[21] K. Raghavachari, Z. Phys. D **12**, 61 (1989).

[22] L. Adamowicz, Chem. Phys. Lett. **182**, 45 (1991).

[23] M. Vala, T. M. Chandrasekhar, J. Szczepanski, and R. Pellow, High Temp. Sci. **27**, 19 (1990).

[24] R. J. Van Zee, R. F. Ferrante, K. J. Zeringue, W. Weltner, Jr., and D. W. Ewing, J. Chem. Phys. **88**, 3465 (1988).

[25] H. Heldman, D. Kella, E. Malkin, E. Miklazky, Z. Vager, J. Zajfman, and R. Naaman, J. Chem. Soc. Faraday Trans. **86**, 2469 (1990); M. Algranati, H. Heldman, D. Kella, E. Malkin, E. Miklazky, R. Naaman, Z. Vager, and J. Zajfman, Isr. J. Chem. **30**, 79 (1990).

[26] P. L. Jones, R. D. Mead, B. E. Kohler, S. D. Rosner, and W. C. Lineberger, J. Chem. Phys. **73**, 4419 (1980); U. Hefter, R. D. Mead, P. A. Schulz, and W. C. Lineberger, Phys. Rev. A **28**, 1429 (1983).

[27] P. A. Schulz, R. D. Mead, P. L. Jones, and W. C. Lineberger, J. Chem. Phys. **77**, 1153 (1982).

[28] G. F. Gantefor, D. M. Cox, and A. Kaldor, J. Chem. Phys. **94**, 854 (1991).

[29] G. F. Gantefor, D. M. Cox, and A. Kaldor, J. Chem. Phys. **96**, 4102 (1992).

[30] T. N. Kitsopoulos, I. M. Waller, J. G. Loeser, and D. M. Neumark, Chem. Phys. Lett. **159**, 300 (1989); T. N. Kitsopoulos, C. J. Chick, Y. Zhao, and D. M. Neumark, J. Chem. Phys. **95**, 1441 (1991).

[31] T. G. Dietz, M. A. Duncan, D. E. Powers, and R. Z. Smalley, J. Chem. Phys. **74**, 6511 (1981).

[32] J. M. B. Bakker, J. Phys. E **6**, 785 (1973); **7**, 364 (1974).

[33] K. Müller-Dethlefs, M. Sander, and E. W. Schlag, Z. Naturforsch. **39a**, 1089 (1984); Chem. Phys. Lett. **12**, 291 (1984); K. Müller-Dethlefs and E. W. Schlag, Annu. Rev. Phys. Chem. **42**, 109 (1991).

[34] E. P. Wigner, Phys. Rev. **73**, 1003 (1948).

[35] R. Spohr, P. M. Guyon, W. A. Chupka, and J. Berkowitz, Rev. Sci. Instrum. **42**, 1872 (1971).

[36] T. Baer, W. B. Peatman, and E. W. Schlag, Chem. Phys. Lett. **4**, 243 (1969).

[37] J. D. Watts and R. J. Bartlett, J. Chem. Phys. **97**, 3445 (1992).

[38] G. Herzberg, *Electronic Spectra of Polyatomic Molecules* (Van Nostrand, Princeton 1967), Vol. III, p. 176.

[39] K. Raghavachari and J. S. Binkley, J. Chem. Phys. **87**, 2191 (1987).

[40] A. Van Orden and R. J. Saykally (private communication), March, 1992.

[41] J. Kurtz and L. Adamowicz, Astrophys. J. **370**, 784 (1991).

[42] W. C. Lineberger and T. A. Patterson, Chem. Phys. Lett. **13**, 40 (1972).

[43] E. A. Brinkman, E. Günther, and J. I. Brauman, J. Chem. Phys. **95**, 6195 (1991).

[44] U. Fano, Phys. Rev. **124**, 1866 (1961).

[45] R. S. Berry, J. Chem. Phys. **45**, 1228 (1966); R. S. Berry and S. E. Nielson, Phys. Rev. **1**, 395 (1970).

[46] J. N. Bardsley, Chem. Phys. Lett. **1**, 229 (1967).

This article is copyrighted as indicated in the article. Reuse of AIP content is subject to the terms at: http://scitation.aip.org/termsconditions. Downloaded to IP: 129.174.21.5 On: Wed, 24 Dec 2014 14:15:05

[47] J. Simons, J. Am. Chem. Soc. **103**, 3971 (1981).
[48] P. K. Acharya, R. A. Kendall, and J. Simons, J. Am. Chem. Soc. **106**, 3402 (1984).
[49] R. D. Mead, K. R. Lykke, W. C. Lineberger, J. Marks, and J. I. Brauman, J. Chem. Phys. **81**, 4883 (1984); K. R. Lykke, R. D. Mead, and W. C. Lineberger, Phys. Rev. Lett. **52**, 2221 (1984).
[50] K. R. Lykke, D. M. Neumark, T. Andersen, V. J. Trapa, and W. C. Lineberger, J. Chem. Phys. **87**, 6842 (1987).
[51] K. J. Taylor, C. Jin, J. Conceica, L. Wang, O. Cheshnovsky, B. R. Johnson, P. J. Nordlander, and R. E. Smalley, J. Chem. Phys. **93**, 7515 (1990).
[52] W. R. Garrett, Phys. Rev. A **3**, 961 (1971), and references therein.

This article is copyrighted as indicated in the article. Reuse of AIP content is subject to the terms at: http://scitation.aip.org/termsconditions. Downloaded to IP: 129.174.21.5 On: Wed, 24 Dec 2014 14:15:05